JACS
JOURNAL OF THE AMERICAN CHEMICAL SOCIETY
Article
pubs.acs.org/JACS

Theory and X-ray Absorption Spectroscopy for Aluminum Coordination Complexes – Al K-Edge Studies of Charge and Bonding in (BDI)Al, (BDI)AlR_2, and (BDI)AlX_2 Complexes

Alison B. Altman,[†,‡] C. D. Pemmaraju,[‡] Clément Camp,[†] John Arnold,*[,†,‡] Stefan G. Minasian,*[,‡] David Prendergast,*[,§] David K. Shuh,*[,‡] and Tolek Tyliszczak[∥]

[†]Department of Chemistry, University of California, Berkeley, California 94720, United States
[‡]Chemical Sciences Division, [§]Molecular Foundry, and [∥]Advanced Light Source, Lawrence Berkeley National Laboratory, Berkeley, California 94720, United States

Supporting Information

ABSTRACT: Polarized aluminum K-edge X-ray absorption near edge structure (XANES) spectroscopy and first-principles calculations were used to probe electronic structure in a series of (BDI)Al, (BDI)AlX_2, and (BDI)AlR_2 coordination compounds (X = F, Cl, I; R = H, Me; BDI = 2,6-diisopropylphenyl-β-diketiminate). Spectral interpretations were guided by examination of the calculated transition energies and polarization-dependent oscillator strengths, which agreed well with the XANES spectroscopy measurements. Pre-edge features were assigned to transitions associated with the Al 3p orbitals involved in metal–ligand bonding. Qualitative trends in Al 1s core energy and valence orbital occupation were established through a systematic comparison of excited states derived from Al 3p orbitals with similar symmetries in a molecular orbital framework. These trends suggested that the higher transition energies observed for (BDI)AlX_2 systems with more electronegative X^{1-} ligands could be ascribed to a decrease in electron density around the aluminum atom, which causes an increase in the attractive potential of the Al nucleus and concomitant increase in the binding energy of the Al 1s core orbitals. For (BDI)Al and (BDI)AlH_2 the experimental Al K-edge XANES spectra and spectra calculated using the eXcited electron and Core–Hole (XCH) approach had nearly identical energies for transitions to final state orbitals of similar composition and symmetry. These results implied that the charge distributions about the aluminum atoms in (BDI)Al and (BDI)AlH_2 are similar relative to the (BDI)AlX_2 and (BDI)$AlMe_2$ compounds, despite having different formal oxidation states of +1 and +3, respectively. However, (BDI)Al was unique in that it exhibited a low-energy feature that was attributed to transitions into a low-lying p-orbital of b_1 symmetry that is localized on Al and orthogonal to the (BDI)Al plane. The presence of this low-energy unoccupied molecular orbital on electron-rich (BDI)Al distinguishes its valence electronic structure from that of the formally trivalent compounds (BDI)AlX_2 and (BDI)AlR_2. The work shows that Al K-edge XANES spectroscopy can be used to provide valuable insight into electronic structure and reactivity relationships for main-group coordination compounds.

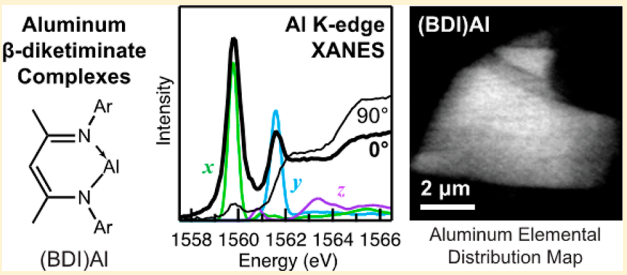

INTRODUCTION

Aluminum is the most abundant metal in the earth's crust and an essential component of many scientific and large-scale industrial processes. With steady improvements in production efficiency and manufacturing methods, aluminum metal is likely to replace other metals in applications owing to its desirable physical and mechanical properties, low cost, relatively low toxicity, and recyclability.[1] At present, intermetallics, alloys, and compounds of aluminum are widely employed in d- and f-block materials science,[2] nanomaterials synthesis,[3,4] and solid-state lighting devices.[5] Aluminum coordination compounds are also valued participants in chemical transformations where they can activate substrates during Friedel–Crafts alkylations and during Ziegler–Natta olefin polymerizations where aluminum organometallic derivatives such as methylaluminoxane are commonly used as cocatalysts.[6,7] More recently, aluminum-containing molecules have been paired with phosphines possessing sterically demanding ligands to activate CO_2 for reduction to CO.[8,9] In many of these systems, aluminum can be regarded as a redox inert, electropositive, Lewis-acidic metal with a formal +3 charge and small ionic radius. However, this simple model has been found inadequate for describing electronic structure in several instances. For example, low-valent aluminum coordination compounds,[10−17] often with double or triple bonds involving the aluminum atoms,[18−20] have been isolated and characterized in depth by a variety of techniques including NMR[21−23] and reactivity studies.[24−28] Together with computational[29−35] and spectroscopic[36−41] techniques, this has led to improved models of aluminum electronic structure grounded in

Received: June 5, 2015
Published: August 10, 2015

DOI: 10.1021/jacs.5b05854
J. Am. Chem. Soc. 2015, 137, 10304−10316

molecular orbital theory. Some compounds containing aluminum in the +1 formal oxidation state exhibit singlet carbene character: they possess a nonbonding pair of electrons and can behave as Lewis bases,[42,43] and can undergo oxidative reactions readily with organic and main-group molecules.[29,42,44−48] More recent work by Nikonov,[49] Fischer,[50] and Crimmin[51] has shown that the oxidative reactions are reversible, allowing for reductive elimination from an Al compound with a +3 formal oxidation state to form an Al compound with a +1 formal oxidation state. Along similar lines, work by Berben and co-workers has shown that aluminum compounds supported by noninnocent ligands have tunable reduction potentials based on the electronics of the ancillary ligands, demonstrating reactivity and physical properties that were previously reserved for redox-active d-block transition metals.[52−57] Clearly, more powerful analytical techniques are needed to evaluate current models of electronic structure and understand the diverse and expanding role aluminum plays across chemical synthesis, materials science, and technology.

Metal K-edge X-ray absorption near-edge structure (XANES) spectroscopy is a widely used technique for probing changes in geometry, ligand environment, and oxidation state in coordination compounds and materials.[58−63] For d-block metals, K-edge XANES probes both dipole-allowed transitions from the core 1s → empty *n*p orbitals as well as weaker quadrupole-allowed transitions to the *n*d orbitals (*n* = principle quantum number) from which most bonding information is derived.[64] In principle, aluminum K-edge XANES can also be used to extract valuable information because the Al 3p valence orbitals are directly involved in bonding. However, earlier efforts to measure, model, and interpret Al K-edge XANES data have been thwarted by several obstacles. In large part, experiments using aluminum K-edge XANES have been limited[65−72] because the intermediate energy regime that includes the Al K-edge (ca. 1555−1585 eV)[73] has historically been difficult to access at many synchrotron radiation facilities and beamlines. As a result, Al K-edge measurements are often subject to poor energy resolution, reduced X-ray photon flux, and incompatible sample preparation methodologies that can result in self-absorption and saturation effects. Furthermore, there are few series of stable aluminum compounds that exhibit a wide range of ligand environments and formal oxidation states while preserving structural similarities that are desirable for systematic spectroscopic studies.

The results provided herein show that these challenges could be overcome for a series of molecular aluminum complexes with 2,6-diisopropylphenyl-*β*-diketiminate (BDI) supporting ligands. This ligand system was chosen because it provided access to a series of structurally related (BDI)AlR_2 and (BDI)AlX_2 complexes (R = H, Me; X = F, Cl, I) in addition to (BDI)Al, which is a rare example in the literature of an isolable monomeric aluminum(I) complex that is stable at room temperature.[13,74−76] The work took advantage of several recent advances in synchrotron radiation instrumentation including the development of scanning transmission X-ray microscopes (STXMs) and diffraction grating monochromators capable of reaching more than 2 keV, which are now installed at many beamlines.[77−80] Pre-edge transitions in the aluminum K-edge XANES spectra of crystalline samples were experimentally identified through an in-depth comparison of the polarization dependence of transition intensities. The assignments were further confirmed using first-principles density functional theory (DFT) calculations within the eXcited electron and Core−Hole (XCH) approach.[81] Comparison of transitions into comparable excited states of (BDI)Al and (BDI)AlH_2 revealed only slight differences in electron density on the Al atoms relative to (BDI)$AlMe_2$ and (BDI)AlX_2 (X = F, Cl, I), which has important implications for understanding the reductive and oxidative reactivity of aluminum coordination compounds.

EXPERIMENTAL SECTION

General Synthetic Details. All reactions were performed either using standard Schlenk line techniques or in a MBraun inert atmosphere glovebox under a purified nitrogen atmosphere (<0.1 ppm of O_2/H_2O). Hexanes, toluene, diethyl ether (Et_2O), and tetrahydrofuran (THF) were dried and degassed using a commercially available Phoenix Solvent Drying System from JC Meyer Solvent Systems. C_6D_6 and $CDCl_3$ were dried over sodium/benzophenone and CaH_2, respectively, and vacuum transferred to a storage flask before being stored in a drybox. Solution NMR spectra were collected on either Bruker AVB-400, AVQ-400, or DRX-500 spectrometers at ambient temperature. ^{1}H NMR chemical shifts (δ in ppm) were calibrated to residual solvent peaks. All reagents were acquired from commercial sources and used without further purification, with the exception of iodine and aluminum trichloride, which were purified by sublimation, and $LiAlH_4$, which was purified by extraction with dry Et_2O. (BDI)H,[82] (BDI)Li·Et_2O,[83] (BDI)$AlMe_2$,[74] (BDI)AlI_2,[13] (BDI)Al,[13] (BDI)AlF_2,[76] and (BDI)$AlCl_2$[75] were synthesized according to literature procedures and characterized using single-crystal X-ray diffraction and/or ^{1}H and ^{27}Al NMR prior to use. The crystal structure of (BDI)AlI_2, reported in the Supporting Information, was determined to allow for comparison of its metrical parameters with the (BDI)AlX_2 analogues. ^{27}Al NMR has been used previously to compare changes in Al coordination number and oxidation state and to determine thermodynamic parameters.[21,84] Chemical shifts for the formally Al(III) species are consistent with previous results and generally fell within the known range of 180 to 80 ppm for four-coordinate aluminum complexes (Table 1).[21,84,85]

Table 1. ^{27}Al NMR Chemical Shifts (δ) Determined for Each of the Synthesized Compounds

compound	^{27}Al NMR shift (ppm)
(BDI)Al	[a]
(BDI)$AlMe_2$	160.0
(BDI)AlH_2	130.2
(BDI)$AlCl_2$	100.7
(BDI)AlI_2	84.0
(BDI)AlF_2	67.0[b]

[a]No ^{27}Al resonance was observed.[13] [b]Resonance is coincident with a large background resonance from the instrument.

Synthesis of (BDI)AlH_2. A modified version of a published procedure was used.[86] A mixture of $LiAlH_4$ (0.448 g, 11.8 mmol) and (BDI)H (4.20 g, 10.0 mmol) was suspended in toluene (80 mL). The mixture was heated at 90 °C for 5 days. The solution was then filtered, concentrated to approximately 20 mL by removal of solvent *in vacuo*, and cooled to −30 °C resulting in formation of a colorless crystalline solid (1.44 g, 32% yield). ^{1}H NMR data matched previously reported literature values.[87]

Sample Preparation and Orientation. Sample preparation and methodology for handling air-sensitive analytes was similar to that described previously.[88−91] Samples were prepared in an argon-filled glovebox by grinding crystals of the analyte into a fine powder with a mortar and pestle and brushing the powder onto a Si_3N_4 membrane (100 nm, Silson) with a fiber. This method arranged a large number of micron-scale crystals in a relatively compact area that were suitable for Al K-edge measurements. A second membrane was placed over the sample, and the edges were sealed together using Hardman Double/Bubble 5 min epoxy.

DOI: 10.1021/jacs.5b05854
J. Am. Chem. Soc. 2015, 137, 10304−10316

Table 2. Relevant Bond Distances (Å) and Angles (deg) of (BDI)Al and (BDI)AlL$_2$ Compounds (L = H, Me, F, Cl, I)

compound	ave Al−N distance (Å)	ave Al−L distance (Å)	N−Al−N angle (deg)	L−Al−L angle (deg)	BDI plane-Al distance (Å)	BDI−BDI plane angle (deg)[a]
(BDI)Al	1.958(2)	–	89.86(8)	–	0.010	15.49
(BDI)AlH$_2$	1.899(1)	1.52(1)	96.41(5)	113(1)	0.006	11.56
(BDI)AlMe$_2$	1.929(9)	1.965(8)	96.2(1)	117.4(1)	0.721	24.59
(BDI)AlF$_2$	1.877(8)	2.52(2)	99.30(6)	107.81(6)	0.001	12.68
(BDI)AlCl$_2$	1.88(1)	2.13(1)	99.36(4)	108.02(2)	0.525	49.82
(BDI)AlI$_2$	1.866(1)	1.652(4)	100.07(6)	108.41(2)	0.600	0

[a]The BDI−BDI plane angle reflects the alignment of molecules within the unit cell between nonsymmetry-related molecules.

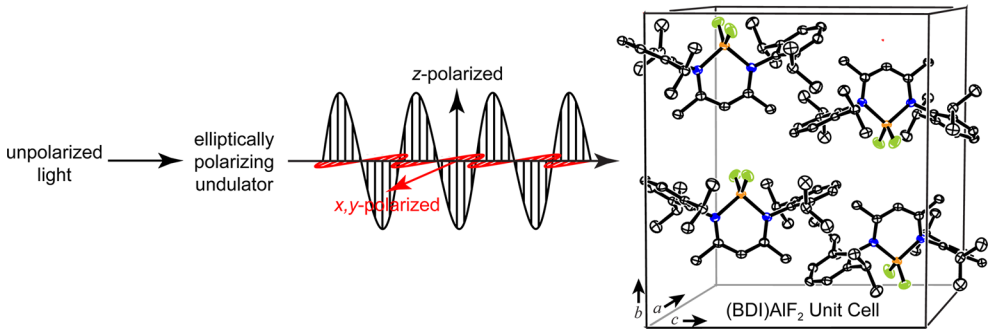

Figure 1. Projection of the crystal structure of (BDI)AlF$_2$ onto the *bc* plane with respect to polarized synchrotron radiation. Thermal ellipsoids are shown with 50% probability, with atoms colored as white (carbon), blue (nitrogen), orange (aluminum), and green (fluorine). Hydrogen atoms have been omitted for clarity. Adapted with permission from Singh, S.; Ahn, H.-J.; Stasch, A.; Jancik, V.; Roesky, H. W.; Pal, A.; Biadene, M.; Herbst-Irmer, R.; Noltemeyer, M.; Schmidt, H.-G. *Inorg. Chem.*, **2006**, *45*, 1853−1860. Copyright 2006 American Chemical Society.

All compounds crystallized in the $P2_1/n$ space group or its alternative setting $P2_1/c$ except for (BDI)AlI$_2$ which crystallized in the *P*-1 space group (Figure S1 in the Supporting Information). The unit cells contained two or four formula units, and the planes defined by the BDI ligands were skewed to varying extents (Table 2). Hence, certain aspects of the molecular symmetry of individual molecules were preserved in the crystal lattice packing and resulted in an X-ray absorption dichroism for each of these compounds.

Beamline Characteristics. STXM methodology was similar to that discussed previously.[88−91] Single-energy images and Al K-edge XANES spectra were acquired using the STXM instrument at the Molecular Environmental Science (MES) beamline 11.0.2 at the Advanced Light Source (ALS), which is operated in topoff mode at 500 mA, in a ∼ 0.5 atm He-filled chamber.[92] The beamline uses photons from an elliptically polarizing undulator that delivers photons in the 100−2000 eV energy range to a variable-angle included plane-grating monochromator. For Al K-edge measurements, the photon energy of the high-energy diffraction grating was calibrated to the Al K-edge for a 1000 Å aluminum filter sample (Luxel, inflection point = 1559.0 eV). The maximum energy resolution $E/\Delta E$ was previously determined at better than 7500,[79] which is consistent with the observed standard deviation for spectral transitions of ±0.3 eV determined from comparison of spectral features over multiple particles and beam runs. For these measurements, the X-ray beam was focused with a zone plate onto the sample, and the transmitted light was detected. The spot size and spectral resolution were determined from characteristics of the 25 nm zone plate. Images at a single energy were obtained by raster-scanning the sample and collecting transmitted monochromatic light as a function of sample position. Spectra at particular regions of interest in the sample image were extracted from the "stack", which is a collection of images recorded at multiple, closely spaced photon energies across the absorption edge.[93] Dwell times used to acquire an image at a single photon energy were 1 or 2 ms per pixel. To quantify the absorbance signal, the measured transmitted intensity (I) was converted to optical density using Beer−Lambert's law: OD = $\ln(I/I_0) = \mu\rho d$, where I_0 is the incident photon flux intensity, d is the sample thickness, and μ and ρ are the mass absorption coefficient and density of the sample material, respectively. Incident beam intensity was measured through the sample-free region of the Si_3N_4 windows. Regions of particles with an absorption of >1.5 OD were omitted to ensure the spectra were in the linear regime of the Beer−Lambert law.

Polarized Al K-edge XANES Spectroscopy Studies. Initial imaging surveys of the samples revealed a large number of crystalline particles that had adopted random orientations on the Si_3N_4 membranes during sample preparation. To determine the nature of any polarization dependence, the EPU was set to horizontal polarization, and spectra were recorded on different crystalline particles until spectra were observed that had maximized or minimized transition intensities. The polarization vector was then rotated by 90° by setting the EPU to vertical, and the Al K-edge XANES measurement was repeated (see Figure 1). Additional spectra were also recorded at intermediate beam polarizations in steps of 10−15° between the limits of 0 and 90°. Relative changes in transition intensities observed in the directionally dependent spectra were compared for measurements on the same particle, which greatly aided spectral assignments. During the STXM experiment, single-energy images showed no signs of radiation damage to the particles, and the polarization dependence of the spectra was reproduced from multiple independent crystallites and beam runs.

Data Analysis. The data were background subtracted using the *MBACK* algorithm in *MATLAB*.[94] Fits for the Al K-edge data were generated using the program IGOR 6.0 and a modified version of EDG_FIT.[95] Spectra were modeled using pseudo-Voigt line shapes consisting of an equal mixture of Gaussian and Lorentzian character as well as a step function with a 1:1 ratio of arctangent and error function contributions.[96] In each case, these analyses provided high-quality fits of the experimental data as reflected by low-correlation coefficients, residual data that deviated slightly from zero, and symmetric residual peaks that matched well with the parent pseudo-Voigt functions. Uncertainty in the transition energies was estimated at ±0.3 eV based on the resolving power of instrument and on the variation in energy of functions comprising the curve fits.

Electronic Structure Calculations. Geometries of all the Al complexes considered were optimized within DFT[97,98] simulations based on a projector augmented wave (PAW)[99] pseudopotential and

DOI: 10.1021/jacs.5b05854
J. Am. Chem. Soc. 2015, 137, 10304−10316

plane-wave basis set framework as implemented in the VASP package.[100] The exchange−correlation energy was treated at the level of the Perdew−Burke−Ernzerhof (PBE)[101] generalized gradient approximation (GGA). Dispersion forces were taken into account using the DFT-D2 approach.[102] In conjunction with a plane-wave energy cutoff of 350 eV, pseudopotentials with the following valence electronic configurations were employed: Al($3s^2 3p^1$), C($2s^2 2p^2$), N($2s^2 2p^3$), H($1s^1$), F($2s^2 2p^5$), Cl($3s^2 3p^5$), I($5s^2 5p^5$). The Brillouin zone was sampled at the Γ point. Geometries were optimized until all forces were smaller than 0.02 eV/Å. Structures so obtained were used in subsequent X-ray absorption spectroscopy simulations.

Al K-edge Spectral Simulations. XANES at the Al K-edge were calculated using the XCH approach.[81] The XCH approach has been described previously in detail.[81,103,104] In this method, the lowest energy X-ray excited state of the system is modeled within an occupation-constrained DFT framework wherein the core-excited atom is described through a core−hole pseudopotential, and the screening due to the excited electron is taken into account self-consistently. Higher lying X-ray excited-state energies are approximated through eigenvalue differences obtained from the Kohn−Sham (KS) spectrum of the lowest energy core-excited state. X-ray transition matrix elements are calculated using Fermi's golden rule and typically for light-element K-edges, within a dipole approximation. The XCH method was utilized as implemented in a development version of the Quantum-Espresso package[105] that provides a plane-wave pseudopotential DFT framework for electronic structure calculations. Ultrasoft pseudopotentials[106] with the same valence electronic configuration as described above were used together with a plane-wave energy cutoff of 25 Ry. To describe 1s core-excited Al in XANES simulations, a core−hole pseudopotential with the electronic configuration $1s^1 2s^2 2p^6 3s^2 3p^2$ was generated. The Brillouin zone was sampled at the zone center during the self-consistent field calculation, but the band structure was interpolated over a uniform Γ-centered 5 × 5 × 5 *k*-point grid using the Shirley interpolation scheme[107] in order to generate spectra.

XANES spectra were obtained both for the molecular crystal unit-cells containing multiple Al complexes as well as for individual molecular units extracted from the optimized crystal geometries. The spectra of molecular crystals differed insignificantly from that of isolated molecular units in the near edge region of interest as shown in Figure S2 in the Supporting Information for the case of (BDI)Al. Therefore, spectra obtained from molecular unit simulations were used in the subsequent analysis as they facilitate a convenient decomposition of the spectrum into contributions from different polarization directions.

Within the XCH approach, the relative energy alignment of XANES spectra corresponding to core-excitations on atoms in different chemical environments is carried out through total energy differences.[103] However, since the method is based on core−hole pseudopotentials and does not explicitly include the energy of core electrons, calibration of the absolute energy position of the calculated spectra with respect to experiment involves a rigid energy shift Δ, which depends on the core-excitation edge being considered.[103] For a wide range of light-element K-edges, the shift Δ may be calculated once for a given excitation-edge based on a reference chemical system, and the same shift can be applied to all XCH spectra calculated at that excitation-edge in different chemical environments.[103,104,108] At the Al K-edge for the complexes in this study, the (BDI)Al complex was used as the reference system and a value of Δ = 1560.27 eV was determined. However, such an alignment scheme led to a systematic red-shift of +0.9 to 1.8 eV in the calculated spectra of all other complexes with respect to experiment, although the spectral line shapes were well reproduced. The discrepancy was traced to a lack of error cancellation in the KS orbital eigenvalues of the lowest unoccupied molecular orbital (LUMO) and higher lying virtual orbitals in the (BDI)AlR_2 and (BDI)AlX_2 systems. KS eigenvalues calculated at the level of semilocal GGA functionals often suffer from significant self-interaction (SI) errors but can nevertheless yield good spectra provided that the relative SI errors cancel.[109] In the present case, the lowest energy XCH reference configuration was based on an Al 1s → BDI π* excitation that had no Al 3p character, and the eigenvalue difference of the LUMO π* state with respect to higher lying states having significant Al 3p character was underestimated by +0.9 to 1.8 eV. Therefore, this led to a systematic underestimation of the energy positions of various Al 3p derived spectral features that lie higher in energy, and it was necessary to align the spectra individually. The energies of the transitions with the greatest oscillator strength in the calculated spectra were set to be equal to the energies of most intense functions used in the curve-fitting analysis of the experimental spectra, which provided energy shifts of +1561.34, +1561.51, +1561.16, +1561.78, +1562.07 eV for the (BDI)AlH_2, (BDI)$AlMe_2$, (BDI)AlI_2, (BDI)$AlCl_2$, and (BDI)AlF_2, respectively.

XCH final state electronic wave functions corresponding to core-excitations into the virtual orbital manifold were approximated by unoccupied KS wave functions obtained from the self-consistent occupation-constrained DFT calculation including the core−hole. Orbital isosurfaces were visualized using VESTA-3.[110]

RESULTS

Ground-State Electronic Structure and Molecular Orbital Description. β-diketiminate groups are frequently employed as ancillary ligands in coordination chemistry because they provide steric stabilization and desirable solubility properties but do not participate in chemical transformations.[111] Aluminum complexes based on the β-diketiminate ligand were selected for this study because they provided access to a series of structurally related (BDI)Al, (BDI)AlR_2, and (BDI)AlX_2 complexes (R = H, Me; X = F, Cl, I) with relatively high symmetries (Figure 2). These materials were analyzed to

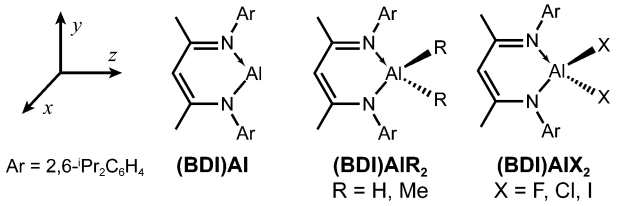

Figure 2. Representation of the (BDI)Al, (BDI)AlR_2, and (BDI)AlX_2 analytes and Cartesian axes system.

evaluate how changing the steric and electronic properties of the reactive R^{1-} or X^{1-} ligands or changing the aluminum formal oxidation state from +1 to +3 affected the aluminum K-edge spectra. In addition, (BDI)Al is the only published example of a monomeric compound with a +1 aluminum formal oxidation state that is stable and isolable at room temperature. This facilitated comparisons with the +3 compounds without introducing Al−Al bonds that are typically found in other Al^{1+} compounds.[112−114]

Before discussing the Al K-edge XANES in detail, it is instructive to provide a framework for evaluating molecular orbital interactions in each complex. Expectations from group theory were derived for (BDI)Al, (BDI)AlR_2 and (BDI)AlX_2 compounds assuming a C_{2v} symmetric geometry. We note that the experimentally determined solid-state structures deviated to varying extents from this idealized coordination environment (Table 2). However, based on this approximation, it was possible to develop the qualitative molecular orbital picture presented in Figure 3 with the relevant core and valence orbitals that were necessary for initial assignment of Al K-edge XANES spectral features. Beginning with the $(BDI)^{1-}$ ligand, the nitrogen 2p orbitals that are directed toward the metal-coordination site combine to form orbitals of a_1 and b_2 symmetry, and those that are perpendicular to the ligand plane have a_2 and b_1 symmetry. In C_{2v} symmetry, the Al 3s

DOI: 10.1021/jacs.5b05854
J. Am. Chem. Soc. 2015, 137, 10304−10316

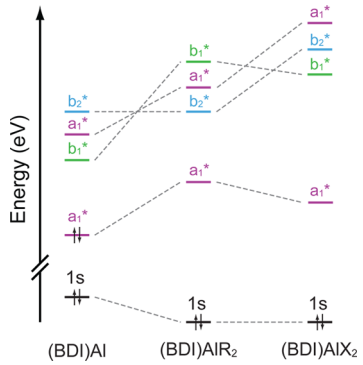

Figure 3. Qualitative molecular orbital diagram showing the relationship between (BDI)Al, (BDI)AlR_2 (R = H, Me), and (BDI)AlX_2 (X = F, Cl, I).

orbital has a_1 symmetry, while the Al 3p orbitals span $b_1 + a_1 + b_2$ symmetries. With these designations the ligand and metal orbitals combine to form an Al 3s-based HOMO of a_1 symmetry, and a low-lying Al 3p-based unoccupied orbital of b_1 symmetry (Figure 4). In this picture, the HOMO is directed

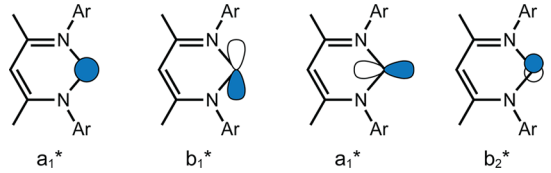

Figure 4. Representation of the Al 3s and 3p orbitals for (BDI)Al.

away from the BDI ligand and is capable of σ-donation, while the vacant b_1* orbital is orthogonal to the (BDI)Al plane and resides at low energy relative to the other antibonding orbitals. In this sense, (BDI)Al is reminiscent of $(C_5Me_5)Al$ in that it is formally isolobal with carbon monoxide and singlet carbenes.[114] The remaining Al 3p orbitals of a_1 and b_2 symmetry interact with ligand orbitals of appropriate symmetry to form unoccupied and antibonding a_1* and b_2* orbitals. It is important to note that the filled Al 3s-based HOMO of a_1 symmetry can also mix with the unoccupied and antibonding Al 3p-based orbital of a_1 symmetry, and previous calculations have suggested that s−p_z mixing is a relevant factor and results in some stabilization of the a_1* orbital.[115] Thus, for the (BDI)Al system, it was predicted that three features would be observed corresponding to transitions into the b_1*, a_1*, and b_2* orbitals at increasing energies as shown in the first column of Figure 3.

Molecular orbitals for each of the (BDI)AlR_2 and (BDI)AlX_2 compounds can be considered a perturbation of those derived for the (BDI)Al compound by first introducing interactions with the reactive R^{1-} and X^{1-} ligands and by then considering the change in Al formal charge and orbital occupation. Group theory shows that the σ donating orbitals on the R^{1-} and X^{1-} ligands combine to form orbitals of a_1 and b_1 symmetry. These have the correct symmetry to interact with and destabilize the (BDI)Al fragment orbitals of a_1 and b_1 symmetry derived above. Interaction with the strictly σ-bonding ligands does not affect the b_2* orbital energy, however some destabilization would be expected for the (BDI)AlX_2 complexes due to π-interactions with the halide ligands. Within this framework, some hybridization of the Al 3s (a_1) and Al 3p_z (a_1) orbitals is possible through s−p mixing. Since the Al 3s orbitals are unoccupied in the (BDI)AlR_2 and (BDI)AlX_2 compounds, this introduces the opportunity for a fourth transition into an additional orbital of a_1 symmetry that is filled for (BDI)Al. Finally, the Al 1s core level is expected to be more stabilized in the (BDI)AlR_2 and (BDI)AlX_2 compounds than in (BDI)Al due to the increase in effective nuclear charge.[64] Thus, it was anticipated that features for compounds with Al^{3+} centers would be higher in energy overall than those observed for the (BDI)Al compound.

Sample Preparation and Imaging. The STXM at the Molecular Environmental Science beamline 11.0.2 of the ALS was used to collect images, elemental maps, and Al K-edge XANES spectra for each of the compounds described above. Samples were prepared in an argon-filled glovebox, and the STXM was filled with a partial atmosphere of helium during acquisition to minimize degradation of the air- and water-sensitive compounds. Figure 5 shows representative contrast images and Al elemental maps of small crystalline particles.

Al K-edge Measurements and Data Reduction. Figure 6 shows the background subtracted and normalized Al K-edge spectra obtained for crystalline samples of (BDI)Al, (BDI)AlR_2, and (BDI)AlX_2 complexes (R = H, Me; X = F, Cl, I). The spectra exhibited some similarities to those observed previously for Al oxides and materials in that a large edge was observed between 1559 and 1566 eV[65,68,116] and different in that several well-resolved pre-edge features were also apparent at low energy. These were associated with dipole-allowed transitions from the Al 1s orbitals into unoccupied orbitals with Al 3p character. Moreover, in many cases aspects of the symmetry of

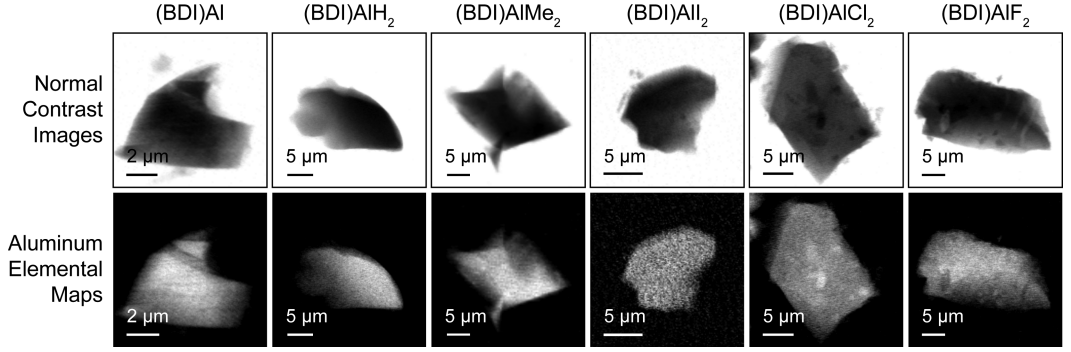

Figure 5. Two images each from the crystallites of (BDI)Al, (BDI)AlR_2, and (BDI)AlX_2 from which Al K-edge XANES spectra were obtained: top row, normal contrast images obtained with photon energies of 1565 eV; bottom row, aluminum elemental maps obtained by subtraction using photon energies of 1565 and 1555 eV.

DOI: 10.1021/jacs.5b05854
J. Am. Chem. Soc. 2015, 137, 10304−10316

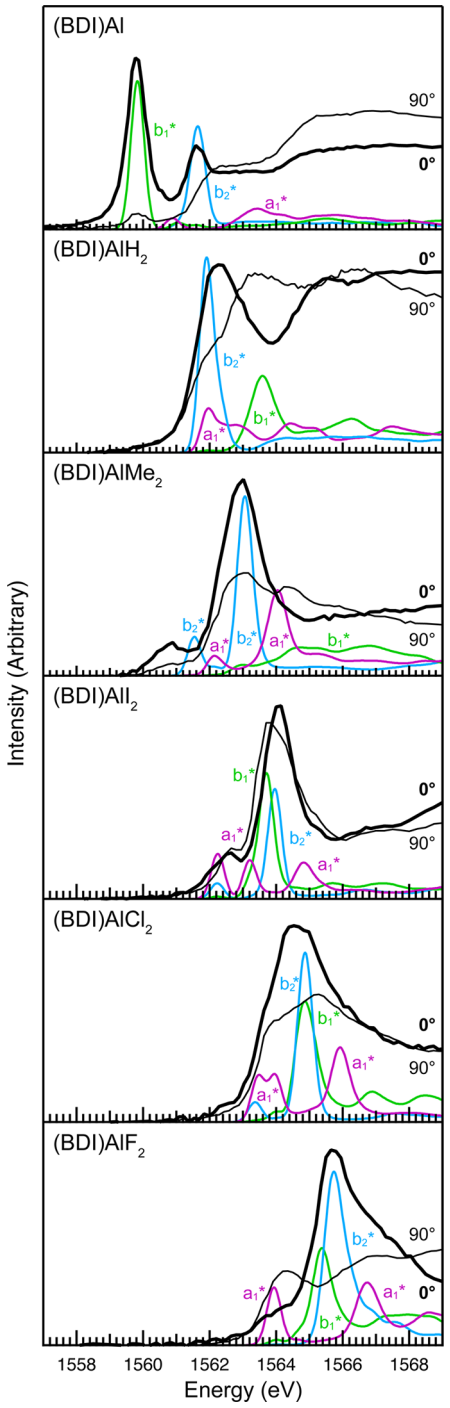

Figure 6. Aluminum K-edge XANES spectra with horizontal (0°, bold black trace) and vertical (90°, fine black trace) light polarization settings. XCH calculated spectra are overlaid on the experimental data and are split into directional components based on the b_1* (green), b_2* (blue), and a_1* (purple) final state orbitals in idealized C_{2v} symmetry.

the individual molecules were preserved by the overall crystal symmetry (see Experimental Section) such that the polarized X-ray beam interacted anisotropically with each particle and relative spectral intensities changed with the changing polarization of the X-ray beam. These changes were consistent with spectral assignments in that features observed at different polarizations were assigned to orbitals of different symmetry.

To accurately determine peak energies, spectra were modeled as previously described (Table 3 and Figures S3–S8 in the Supporting Information).[96] First and second derivatives of the experimental data were used as a guide to derive curve-fitting models and suggested that the pre-edge regions in all spectra were best modeled by 2–4 functions. The curve-fitting models were also examined to ensure consistency for a given analyte regardless of sample orientation or beam polarization. In each case, these analyses provided high-quality fits of the experimental data as reflected by low correlation coefficients, residual data that deviated slightly from zero and symmetric residual peaks that matched well with the parent pseudo-Voigt functions. For $(BDI)AlH_2$, a fully unconstrained deconvolution did not converge with reasonable parameters that were consistent for different polarizations. Therefore, to obtain a realistic and consistent model, the energy of the step function for the horizontally polarized spectrum was constrained to match that for the vertically polarized spectrum. Similarly, to obtain a realistic fit of the horizontal spectrum of $(BDI)AlF_2$, the widths of the functions at 1566.5(3) and 1567.8(3) eV were constrained to less than 0.9 eV.

Table 3. Comparison of Experimental and Calculated Al K-Edge Energies to Given Final State Orbitals in Idealized C_{2v} Symmetry for (BDI)Al, $(BDI)AlR_2$ and $(BDI)AlX_2$ (R = H, Me, X = F, Cl, I)

	final state	transition energy (eV)	
compound	orbital	exptl[a]	calcd[b]
(BDI)Al	b_1	1559.8(2)	1559.8
	a_1	[c]	1560.9
	b_2	1561.7(2)	1561.6
$(BDI)AlH_2$	b_2	1561.9(2)	1561.9
	a_1	1562.8(2)	1563.0[d]
	b_1	1564.5(2)	1563.6
$(BDI)AlMe_2$	b_2	1560.8(2)	1561.5
	a_1	1562.4(2)	1562.1
	b_2	1563.0(2)	1563.0
	a_1	1564.3(2)	1564.0
$(BDI)AlI_2$	a_1	1562.5(2)	1562.3, 1563.2
	b_1	1563.7(2)	1563.7
	b_2	1564.2(2)	1564.0
	a_1	1564.9(2)	1564.8
$(BDI)AlCl_2$	a_1	1563.7(2)	1563.5, 1564.0
	b_2	1564.2(2)	1564.9
	b_1	1565.0(2)	1565.0
	a_1	1565.9(2)	1566.0
$(BDI)AlF_2$	a_1	1564.1(2)	1564.0
	b_1	1565.6(3)	1565.4
	b_2	1565.6(3)	1565.6
	a_1	1566.3(2)	1566.7

[a]Experimental values were determined from the curve fitting analysis (see Experimental Section, Figure 7, and the Supporting Information). [b]Calculated values were based on the energy the XCH calculated transition with the greatest oscillator strength for a given feature. [c]This transition was not resolved in the experimental spectrum. [d]Because orbital mixing in $(BDI)AlH_2$ resulted in a large number of bound-state Al 1s → a_1* transitions, this given value is estimated.

Pre-edge Spectral Assignments. To guide spectral interpretations, the Al K-edge XANES of (BDI)Al, $(BDI)AlR_2$, and $(BDI)AlX_2$ were calculated using an XCH DFT approach. This approach has been successfully applied to other XANES

DOI: 10.1021/jacs.5b05854
J. Am. Chem. Soc. 2015, 137, 10304–10316

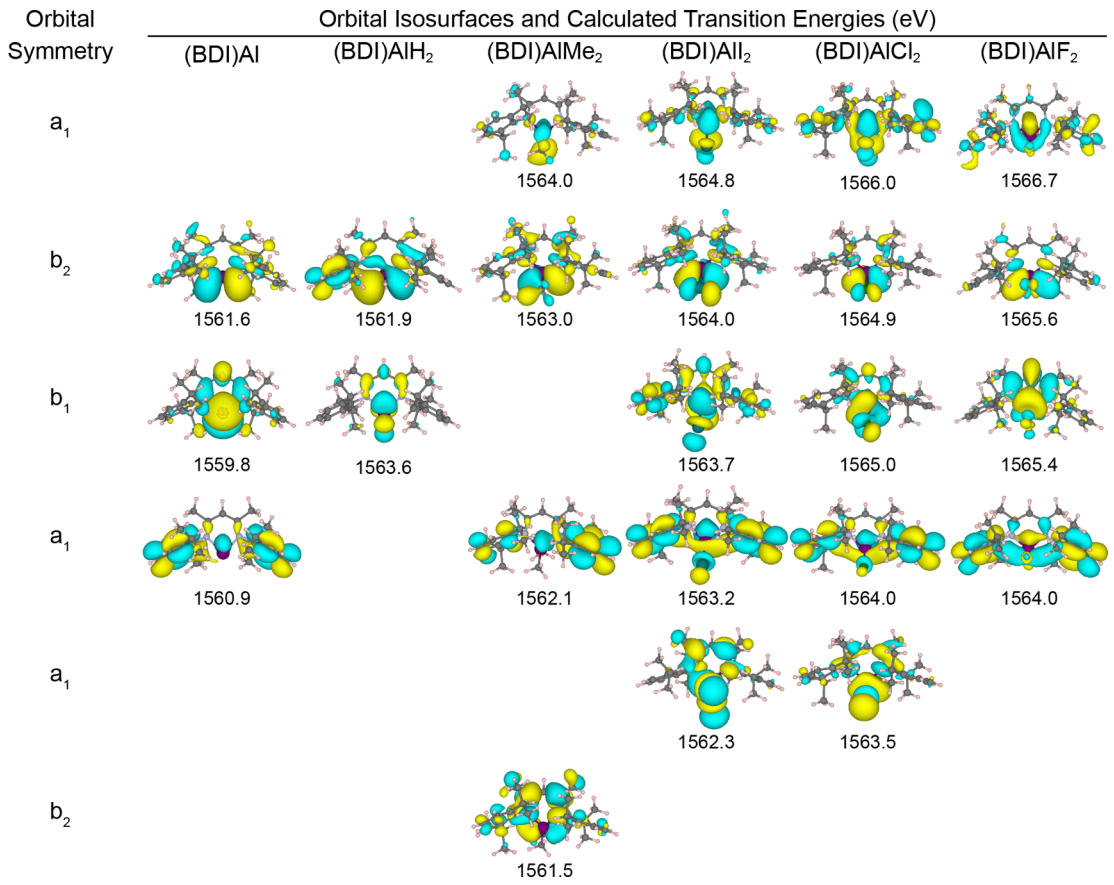

Figure 7. Isosurfaces of the excited states corresponding to the transitions with the greatest oscillator strength for a given feature calculated using the XCH approach.

simulations for s- and p-block inorganic complexes and organic ligands.[108,117−119] Simulations performed on entire unit cells and on individual molecules showed excellent agreement in the pre-edge region; the spectra for individual molecules were deconvoluted into their directional components and are presented in Figure 6. As explained in the Experimental Section, in order to facilitate comparison to experiment, each calculated spectrum has been shifted rigidly along the energy axis by matching the energies of the most intense features in the calculated and experimental spectra. The total calculated spectrum and directionally-dependent components showed good qualitative agreement with the experimental data and results from the curve fitting analyses, respectively. To facilitate assigning spectral features to excited states associated with specific orbitals, these calculations were also used to generate isosurface plots of the final state electronic orbitals that corresponded to each transition. Figure 7 provides plots of the final state orbital isosurfaces that corresponded to the most significant transitions in the (BDI)Al, (BDI)AlR$_2$ and (BDI)AlX$_2$ spectra.

(BDI)Al and (BDI)AlR$_2$ Complexes. For (BDI)Al, two distinct features were observed in the experimental spectrum at 1559.8(2) and 1561.7(2) eV whose intensities decreased significantly when the polarization vector was rotated to 90° (Figure 8). Comparison with the XCH calculations suggested that these features corresponded to transitions into the b_1* and b_2* orbitals, respectively. The Al 1s → b_1* transition for (BDI)Al is significantly lower in energy than the lowest energy feature that was previously reported at 1561.2 eV for [(C$_5$Me$_5$)Al]$_4$ (Al 1s → t_2*),[120] which may reflect the differences in ligand, geometry, or the presence of Al−Al bonds, and may be correlated to differences in the determined Lewis acidity of these compounds.[42,121] The calculations also indicated that a weak transition into the a_1* orbital occurred at 1560.9 eV. However, because Al 1s → Al 3s transitions are dipole forbidden, the a_1* transition intensity resulting primarily from hybridization effects was predicted to be low and was not resolved in the experimental spectrum.

In contrast to (BDI)Al, which exhibited multiple sharp pre-edge features, fewer features stood out in the Al K-edge spectrum of (BDI)AlH$_2$. One broad and asymmetric feature was observed near 1562 eV, and after rotating the polarization vector another feature was resolved at higher energy near 1564 eV. The asymmetric feature near 1562 eV was modeled with two functions at 1561.9(2) and 1562.8(2) eV, while the higher energy feature was modeled with one function centered at 1564.5(2) eV. As described for (BDI)Al, the calculations ascribed the low-energy feature centered near 1561.9(2) eV and the high-energy feature at 1564.5(2) eV to transitions from the Al 1s core level to orbitals with b_2* and b_1* character, respectively. In addition, the function at 1562.8(2) eV was assigned to a transition into an orbital with a_1* character.

The experimental (BDI)AlMe$_2$ spectra contained several features that were modeled with three well-resolved functions at 1560.8(2), 1562.4(2), and 1563.0(2) eV and one broad function at higher energy near 1564.3(2) eV. The polarization study and XCH calculations revealed that the transitions corresponding to the functions at 1560.8(2) eV and 1563.0(2) eV were polarized perpendicularly to the transitions corresponding to the functions at 1562.4(2) and 1564.3(2) eV (See

DOI: 10.1021/jacs.5b05854
J. Am. Chem. Soc. 2015, 137, 10304−10316

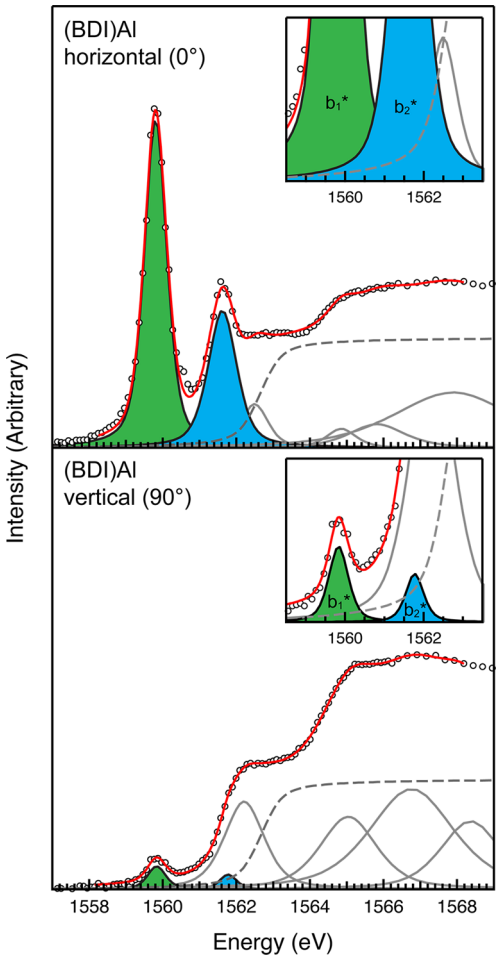

Figure 8. Al K-edge XANES spectra (STXM) experimental data for (BDI)Al at perpendicular light polarization settings (black circles). Pseudo-Voigt functions used to model pre-edge features (blue and green traces), step-function used to model the edge (dashed gray trace), and pseudo-Voigt functions used to model postedge features (solid gray traces) summed to generate the curve fits (red traces). The inset shows the pre-edge features over a smaller energy range with the final state orbital labels corresponding to the transition assigned to each feature. Refer to the Supporting Information for plots of the curve-fitting analysis for (BDI)AlF_2, (BDI)$AlCl_2$, (BDI)AlI_2, (BDI)-AlH_2, and (BDI)$AlMe_2$.

Table 3 for XCH values). Examination of the calculated isosurfaces for each of the final state orbitals corresponding to the functions at 1560.8(2) and 1563.0(2) eV indicated that both were best described as having b_2* character (*y*-polarized). This splitting was not predicted from the simple group theory model for (BDI)AlR_2 derived in C_{2v} symmetry, and the calculations indicated that it was caused by breaking of symmetry in the *x*-direction as the $AlMe_2$ fragment sat above the plane of the BDI ligand. This facilitated a non-negligible σ-type interaction with the BDI ligand that was not observed for (BDI)Al or (BDI)AlH_2. The slight underestimation of the splitting between the two b_2* features is attributed to the use of the semilocal GGA functional within the XCH approach. At higher energy, the functions at 1562.4(2) and 1564.3(2) eV were ascribed to two orbitals having a_1* character (*z*-polarized), resulting from mixing between Al 3s and 3p orbitals and the BDI backbone. The simulated spectra also showed two Al 1s → a_1* transitions: one weaker transition centered at 1562.1 eV and another with greater intensity at 1564.0 eV. Al 1s → 3s transitions are dipole forbidden, and the isosurfaces in Figure 7 suggested that this difference in relative intensity may reflect a smaller amount of Al 3p character in the lower energy a_1* orbital. Finally, the calculations indicated that transitions to the b_1* orbital (*x*-polarized) were not resolved as distinct peaks in the experimental spectra, as a possible consequence of the strongly destabilizing interaction between the Al p_x orbitals and Me ligands.

(BDI)AlX_2 Complexes. At first glance, the experimental Al K-edge XANES spectra for the (BDI)AlX_2 complexes resembled the spectra observed for (BDI)$AlMe_2$, in that they contained one intense, asymmetric feature at higher energy and one weaker feature at low energy (resolved as a shoulder in the (BDI)$AlCl_2$ spectrum). The spectrum for (BDI)AlF_2 was modeled with three functions, and changing polarizations indicated that the function at 1565.6(3) eV was polarized perpendicularly to two functions at 1564.1(2) and 1566.3(2) eV. As described for the (BDI)$AlMe_2$ complex, the XCH calculations ascribed the well resolved function at 1564.1(2) and the broader function at 1566.3(2) eV to transitions into orbitals with a_1* character resulting from mixing between Al 3s and 3p orbitals and the BDI and F ligands (*z*-polarized). Relative to (BDI)Al and the (BDI)AlR_2 compounds, the simulated spectra and calculated isosurfaces suggested that both Al 1s to a_1* transitions were allowed for (BDI)AlF_2 due to enhanced Al 3s and 3p hybridization. The calculations also suggested that the main feature was comprised of two closely spaced transitions with maxima at 1565.4 and 1565.6 eV, respectively. The calculated isosurfaces indicated that the transition at 1565.4 eV corresponded to a b_1*-type orbital that was Al−F σ-antibonding, while the slightly higher energy transition at 1565.6 eV was assigned to a transition into a b_2*-type orbital that was Al−F π-antibonding. These transitions could not be separately resolved in the experimental spectra, and incorporating additional pseudo-Voigt functions into the curve fitting models resulted in energies with large errors.

No significant polarization dependence was observed in the experimental spectra of the remaining halides because the individual molecules of (BDI)AlI_2 and (BDI)$AlCl_2$ are not oriented along crystallographic axes within the unit cell. However, each of the XCH calculations supported an interpretation that was analogous to that described for the Al K-edge XANES of (BDI)AlF_2. For example, the lowest energy functions at 1563.7(2) eV for (BDI)$AlCl_2$ (shoulder) and 1562.5(2) eV for (BDI)AlI_2 were ascribed to transitions into a_1*-type orbitals derived from hybridization between the Al 1s and Al $3p_z$. Moving to higher energy, two closely spaced transitions into orbitals of b_1* and b_2* symmetry were predicted and assigned to the functions at 1563.7(2) and 1564.2(2) eV for (BDI)AlI_2 and 1565.0(2) and 1564.2(2) eV for (BDI)$AlCl_2$, respectively.

■ DISCUSSION

Spectral features at the K-edge for first-row transition metals often follow Kunzl's law, in which 1s → 4p transition energies increase with decreases in the 3d-orbital occupation of the absorbing metal atom.[64] In principle, relative changes in the 1s → 3p transition energies recorded at the Al K-edge can also be used to evaluate differences in valence orbital occupation for the (BDI)Al, (BDI)AlR_2, and (BDI)AlX_2 complexes. However, because the Al 3p-orbitals participate in bonding directly, significant differences in the relative order and composition of the unoccupied molecular orbitals are observed with different

DOI: 10.1021/jacs.5b05854
J. Am. Chem. Soc. 2015, 137, 10304−10316

geometries and ligand environments. Hence, it is necessary to compare the energy of "isolobal" transitions to final state orbitals that have similar orbital compositions and symmetries within a molecular orbital framework. In notation adopted for the simplified C_{2v} symmetric representation, transitions to the Al p_y orbitals that have b_2* symmetry meet this criterion and are observed for all six analytes. Because these orbitals are orthogonal to the Al−R and Al−X bonds and are strictly nonbonding with respect to the R^{1-} ligands, they are more likely to reflect changes in Al electron density or bonding with the BDI supporting ligands.

For (BDI)AlX_2 complexes, Al 1s → b_2* transitions are observed in the experimental Al K-edge XANES spectra at increasing energies such that (BDI)AlF_2 > (BDI)$AlCl_2$ ≈ (BDI)AlI_2 (1565.6(3), 1564.2(2), and 1564.2(2) eV for X = F, Cl, and I, respectively). The XCH calculations support this trend, predicting Al 1s → b_2* transitions centered at 1565.6, 1564.9, and 1564.0 eV for X = F, Cl, and I, respectively. Halide ligand π-donation is expected to destabilize the b_2* orbital and increase the energy of the corresponding Al 1s → b_2* transition. However, examination of the isosurfaces provided in Figure 7 shows that the b_2* orbitals had more halide character for (BDI)$AlCl_2$ and (BDI)AlI_2 and approach Al−F nonbonding for (BDI)AlF_2. Hence, the data suggest that the increase in energy of the Al 1s → b_2* transitions for (BDI)AlF_2 is correlated to the increasing electronegativities of the halide ligands. Along these lines, the Al 1s → b_2* transition for (BDI)$AlMe_2$ decreases further to 1563.0(2) eV, which is in agreement with the group electronegativity of 2.3 that is ascribed to Me^{1-} ligands.[122]

Figure 9 plots values for the experimental Al K-edge transitions associated with final state orbitals of a_1, b_1, or b_2

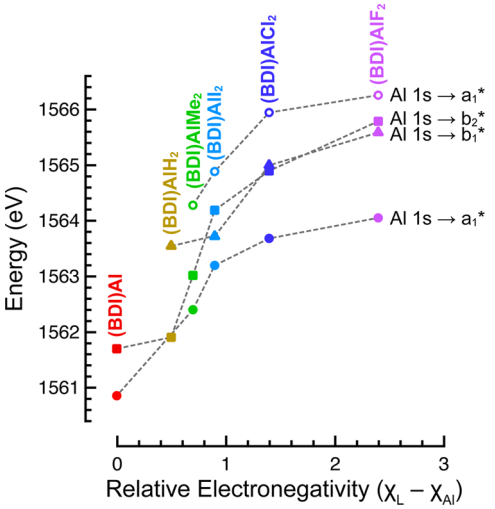

Figure 9. Comparison of the experimental Al K-edge XANES transition energies (eV) from Table 3 and the relative aluminum and ligand electronegativities ($\chi_L - \chi_{Al}$). Calculated transition energies were used in instances when the transitions were poorly resolved in the experimental spectra (see Table 3).

parentage in C_{2v} symmetry relative to Pauling electronegativities (4.0, 3.0, and 2.5 for F, Cl, and I, respectively).[62] Each of the transitions to a_1* (Al−L σ), b_1* (Al−L σ), or b_2* (Al−X π, Al−R nb) final state orbitals shows a trend toward higher energies when more electronegative ligands are incorporated. Hence, the effects of metal−ligand bonding can be accounted for by comparing "isolobal" final states within a molecular orbital framework, which shows that core Al 1s orbital stabilization due to changes in metal electron density plays a significant role in the Al K-edge XAS. This phenomenon has been observed frequently in metal K-edge XANES spectra for d-block transition metals. The shifts in energy have been attributed to metal valence electrons becoming attracted to more electronegative ligands, which effectively decreases the electron density on the metal center and stabilizes the remaining core and valence electrons.[26,63] The generality of this trend for each of the (BDI)Al, (BDI)AlX_2, and (BDI)AlR_2 compounds and for all of the final state orbital symmetries indicates that the Al K-edge XANES transition energies are also driven by changes in electron density at aluminum. In some cases, the range in transition energies can be substantial. For example, the Al 1s → b_2* transition energy for (BDI)AlF_2 compound is 2.6(3) eV higher in energy than the corresponding transition for (BDI)$AlMe_2$, suggesting that significant differences in electron density around the aluminum can occur.

For (BDI)Al, an Al 1s → b_2* transition is observed in the Al K-edge XANES spectrum at 1561.7(2) eV. Despite having different spectral profiles, the curve-fitting analysis suggests that the energy of the Al 1s → b_2* transition is within error of the Al 1s → b_2* transition observed at 1561.9(2) eV for (BDI)AlH_2. In addition, the XCH calculations predict very similar Al 1s → b_2* transition energies of 1561.6 and 1561.9 eV for (BDI)Al and (BDI)AlH_2, respectively. Compared with the higher energy Al 1s → b_2* transitions observed for (BDI)$AlMe_2$ and the (BDI)AlX_2 compounds, the close correspondence between these transitions suggests that the nominal charge at Al and bonding with the BDI supporting ligands is similar for (BDI)Al and (BDI)AlH_2, despite having very different formal charges of +1 and +3, respectively. To further explore this surprising result, the Al 1s core-level binding energies as well as the unoccupied Al projected density-of-states were analyzed in both complexes. The Al 1s → b_2* X-ray transition energy can be decomposed into a noninteracting term equal to the difference in the 1s and b_2* single-particle energy levels and an exciton binding energy. Differences in the Al 1s core-level binding energies are expected to reflect changes in the local electron density environment around the Al atom, while differences in the energy position of the b_2* orbital in the unoccupied manifold should indicate changes in Al bonding to the ligands. The Al 1s core-level binding energies in the two complexes were determined from pseudopotential DFT total energy differences. The Al 1s core-level binding energy in a molecular complex ε_{1s}^{mol} is given by

$$\varepsilon_{1s}^{mol} = \{[E_{FCH,PP}^{mol} - E_{GS,PP}^{mol}] - [E_{FCH,PP}^{atom} - E_{GS,PP}^{atom}]\} + \Delta_{CL}$$

where $E_{FCH,PP}^{mol}$, $E_{GS,PP}^{mol}$, $E_{FCH,PP}^{atom}$, $E_{GS,PP}^{atom}$ represent pseudopotential based total energies of the Al 1s core-ionized molecular ion, the molecular ground state, an isolated 1s core-ionized Al ion, and an isolated Al atom in the ground state, respectively, while Δ_{CL} represents a fixed empirical energy calibration term consistent with the rigid shift Δ applied to the XANES spectrum of (BDI)Al. The abbreviations FCH, GS, PP, and CL stand for full core−hole, ground state, pseudopotential, and core level, respectively. Similarly, the single-particle energy of the b_2* orbital $\varepsilon_{b_2^*}$ was approximated as

$$\varepsilon_{b_2^*} = -EA + (\epsilon_{b_2^*}^{KS} - \epsilon_{LUMO}^{KS})$$

DOI: 10.1021/jacs.5b05854
J. Am. Chem. Soc. 2015, 137, 10304−10316

where EA is the electron affinity determined in a ΔSCF calculation, and $\epsilon^{KS}_{b_2^*}$, ϵ^{KS}_{LUMO} are the ground-state Kohn–Sham eigenvalues of the b_2* and LUMO orbitals, respectively. The calculated Al 1s and b_2* single-particle energies are shown in Table 4, and the unoccupied ground-state DOS as well as the ground-state isosurfaces for the lowest b_2* state are presented in Figure 10.

Table 4. Single-Particle Energies of the Al 1s Core Levels (ϵ^{mol}_{1s}) and Unoccupied b_2* Orbitals

	ε^{mol}_{1s} (eV)	$\varepsilon_{b_2^*}$ (eV)
(BDI)Al	−1564.26	1.960
(BDI)AlH_2	−1564.30	1.994

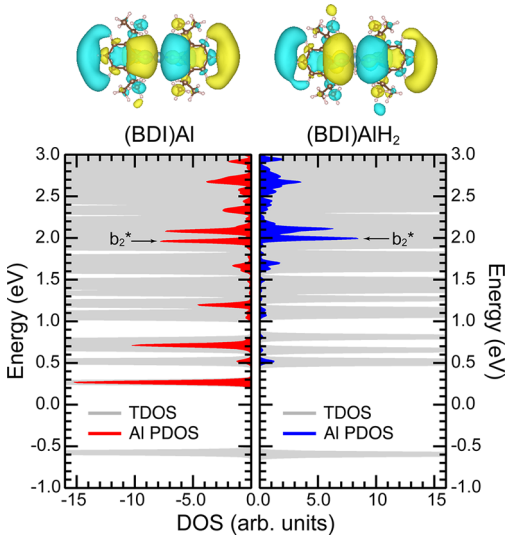

Figure 10. Total (gray) and Al projected (red, blue) unoccupied density-of-states and ground-state orbital isosurfaces for the lowest single particle b_2* state for (BDI)Al and (BDI)AlH_2 complexes.

Remarkably, both the Al 1s core-level and unoccupied b_2* single-particle energies in (BDI)Al and (BDI)AlH_2 are similar, differing by no more than 40 meV, in spite of the very different formal charges on Al. Test calculations employing hybrid-DFT functionals (not shown) confirmed the robustness of this result with respect to DFT functional. The calculations therefore support the experimental results and the interpretation that the ligand field environment induces similar charges for the aluminum atoms in both (BDI)Al and (BDI)AlH_2. This finding is consistent with the generally accepted model that main group elements form covalently bonded hydrides, relative to transition-metal hydrides that can have either more hydridic or more protic character.[123] Additional spectroscopic and theoretical experiments that directly probe the core-state binding energies in (BDI)Al, (BDI)AlX_2, (BDI)AlR_2 and other aluminum coordination compounds are needed to test the limits of this interpretation.

SUMMARY AND CONCLUSIONS

The application of X-ray spectroscopies to probe electronic structure in main-group coordination compounds represents a long-standing experimental challenge. The results of this study show that polarized Al K-edge XANES spectroscopy combined with theory can be used to identify experimental trends that support a detailed picture of σ- and π-bonding interactions between the aluminum metal and associated ligands. Pre-edge features associated with transitions involving the three Al 3p orbitals were observed in the polarized Al K-edge XANES spectra of (BDI)Al, (BDI)AlX_2, and (BDI)AlR_2 (X = F, Cl, I; R = H, Me) and were assigned with the aid of XCH calculations. Metal–ligand bonding played a significant role in establishing the relative energies and ordering of molecular orbitals probed by the 1s → 3p transitions; significant differences were observed depending on the σ- and π-bonding abilities of the X^{1-} and R^{1-} ligands.

By comparing transitions into excited states with similar orbital compositions and symmetries within a molecular orbital framework, it was possible to identify differences in core orbital energies and valence orbital occupation across the series of (BDI)Al, (BDI)AlR_2 and (BDI)AlX_2 complexes while accounting for changes in the ligand environment. The observed transition energies primarily reflected a change in the electron density on Al in the presence of ligands with different electronegativities. This analysis indicated that the charge distribution on aluminum in (BDI)Al was nearly identical to the charge distribution on (BDI)AlH_2, despite having very different valence orbital occupations and formal oxidation states of +1 and +3, respectively. However, (BDI)Al also exhibited a low-energy feature that was attributed to a transition into an unoccupied b_1* orbital, which is best described as a vacant, low-energy Al 3p-orbital that is orthogonal to the (BDI)Al plane. This has important implications for the novel reactivity of (BDI)Al and is a distinguishing aspect of the electronic structure of (BDI)Al relative to (BDI)AlX_2 and (BDI)AlR_2. The combination of theory and XANES spectroscopy in this instance provided insight regarding the nature of Al σ- and π-bonding in specific molecular orbitals that could not be obtained from ^{27}Al NMR spectroscopy or analysis of metrical parameters obtained by single-crystal X-ray diffraction. However, Al K-edge XANES spectroscopy could become a powerful complement to ^{27}Al NMR, which is also sensitive to a range of factors including formal charge and the nature of bonding ligands, their geometry, and coordination number.[21−23,124,125] Studies on a wider range of aluminum molecules and extended solids are needed to explore possible correlations between observables provided by the two techniques.

Whereas first-row transition metals can adopt a range of oxidation states under normal conditions, the $Al^{3+} + 2e^- \rightarrow Al^{1+}$ reduction generally requires strong chemical reducing agents. These studies support the recently observed reversible hydride-transfer reactivity between the (BDI)Al and (BDI)AlH_2 complexes and justify the accessibility of two-electron reductive elimination pathways at aluminum centers.[49,50] This work may impact efforts to destabilize or regenerate aluminum hydrides, which are utilized as reducing agents and hydride sources during organic transformations[126] and as media for hydrogen storage.[127−130] Additional studies to assess the utility of Al K-edge XANES spectroscopy in other hydride systems are underway.

ASSOCIATED CONTENT

Supporting Information

The Supporting Information is available free of charge on the ACS Publications website at DOI: 10.1021/jacs.5b05854.

Background-subtracted and normalized X-ray absorption data and plots of the curve fitting analyses (PDF)

DOI: 10.1021/jacs.5b05854
J. Am. Chem. Soc. 2015, 137, 10304−10316

Crystallographic data (CIF)

AUTHOR INFORMATION

Corresponding Authors

*arnold@berkeley.edu
*sgminasian@lbl.gov
*dgprendergast@lbl.gov
*dkshuh@lbl.gov

Notes

The authors declare no competing financial interest.

ACKNOWLEDGMENTS

A.B.A. acknowledges support by a Department of Energy (DOE) Integrated University Program Fellowship at the University of California, Berkeley. J.A., S.G.M. and D.K.S. were supported by the Director, Office of Science, Office of Basic Energy Sciences, Division of Chemical Sciences, Geosciences, and Biosciences Heavy Element Chemistry Program of the U.S. DOE at LBNL under contract no. DE-AC02-05CH11231. The theory work of C.D.P. and D.P. was supported through a User Project at the Molecular Foundry, LBNL. Calculations were performed on the Cray XE6 Hopper computer at the National Energy Research Scientific Computing Center (NERSC-LBNL) and Molecular Foundry computing resources, Nano and Vulcan, managed by the High Performance Computing Services Group of LBNL. The ALS and T.T. were supported by the Director, Office of Science, Office of Basic Energy Sciences, of the U.S. DOE under contract no. DE-AC02-05CH11231 at LBNL. Research at Beamline 11.0.2 at the ALS was supported by the Director, Office of Science, Office of Basic Energy Sciences, Division of Chemical Sciences, Geosciences, and Biosciences Condensed Phase and Interfacial Molecular Sciences Program of the U.S. DOE at LBNL under contract no. DE-AC02-05CH11231.

REFERENCES

(1) *U.S. Energy Requirements for Aluminum Production: Historical Perspective, Theoretical Limits, and Current Practices*; U.S. Department of Energy: Washington, DC, 2007.
(2) Jullien, R.; Coqblin, B. *J. Phys., Lett.* **1974**, *35*, 197.
(3) Meza, L. R.; Das, S.; Greer, J. R. *Science* **2014**, *345*, 1322.
(4) Kim, S.-H.; Kim, H.; Kim, N. J. *Nature* **2015**, *518*, 77.
(5) Taniyasu, Y.; Kasu, M.; Makimoto, T. *Nature* **2006**, *441*, 325.
(6) Chen, E. Y. X.; Marks, T. J. *Chem. Rev.* **2000**, *100*, 1391.
(7) Zurek, E.; Ziegler, T. *Prog. Polym. Sci.* **2004**, *29*, 107.
(8) Ménard, G.; Stephan, D. W. *J. Am. Chem. Soc.* **2010**, *132*, 1796.
(9) Ménard, G.; Stephan, D. W. *Angew. Chem., Int. Ed.* **2011**, *50*, 8396.
(10) Dohmeier, C.; Loos, D.; Schnöckel, H. *Angew. Chem., Int. Ed.* **1996**, *35*, 129.
(11) Downs, A. *Coord. Chem. Rev.* **1999**, *189*, 59.
(12) Power, P. P. *Chem. Rev.* **1999**, *99*, 3463.
(13) Cui, C.; Roesky, H. W.; Schmidt, H.-G.; Noltemeyer, M.; Hao, H.; Cimpoesu, F. *Angew. Chem., Int. Ed.* **2000**, *39*, 4274.
(14) Roesky, H. W.; Kumar, S. S. *Chem. Commun.* **2005**, 4027.
(15) Dagorne, S.; Atwood, D. A. *Chem. Rev.* **2008**, *108*, 4037.
(16) Nagendran, S.; Roesky, H. W. *Organometallics* **2008**, *27*, 457.
(17) González-Gallardo, S.; Bollermann, T.; Fischer, R. A.; Murugavel, R. *Chem. Rev.* **2012**, *112*, 3136.
(18) Power, P. P.; Moezzi, A.; Pestana, D. C.; Petrie, M. A. *Pure Appl. Chem.* **1991**, *63*, 859.
(19) Wright, R. J.; Brynda, M.; Power, P. P. *Angew. Chem., Int. Ed.* **2006**, *45*, 5953.
(20) Rivard, E.; Power, P. P. *Inorg. Chem.* **2007**, *46*, 10047.
(21) Gauss, J.; Schneider, U.; Ahlrichs, R. *J. Am. Chem. Soc.* **1993**, *115*, 2402.
(22) Schurko, R. W.; Hung, I.; Macdonald, C. L. B.; Cowley, A. H. *J. Am. Chem. Soc.* **2002**, *124*, 13204.
(23) Bono, D.; Hartig, J.; Huber, M.; Schnöckel, H.; de Jongh, L. J. *J. Cluster Sci.* **2007**, *18*, 319.
(24) Cowley, A. H.; Gabbai, F. P.; Isom, H. S.; Decken, A. *J. Organomet. Chem.* **1995**, *500*, 81.
(25) Weiss, J.; Stetzkamp, D.; Nuber, B. *Angew. Chem., Int. Ed.* **1997**, *36*, 70.
(26) Gorden, J. D.; Voigt, A.; Macdonald, C. L. B.; Silverman, J. S.; Cowley, A. H. *J. Am. Chem. Soc.* **2000**, *122*, 950.
(27) Huber, M.; Henke, P.; Schnöckel, H. *Chem. - Eur. J.* **2009**, *15*, 12180.
(28) Dettenrieder, N.; Dietrich, H. M.; Schädle, C.; Maichle-Mössmer, C.; Törnroos, K. W.; Anwander, R. *Angew. Chem., Int. Ed.* **2012**, *51*, 4461.
(29) Ahlrichs, R.; Horn, H.; Ehrig, M. *Chem. Phys. Lett.* **1991**, *183*, 227.
(30) Fink, W. H.; Power, P. P.; Allen, T. L. *Inorg. Chem.* **1997**, *36*, 1431.
(31) Kormos, B. L.; Cramer, C. J. *Inorg. Chem.* **2003**, *42*, 6691.
(32) McKenzie, I.; Percival, P. W.; Clyburne, J. A. C. *Chem. Commun.* **2005**, 1134.
(33) Landis, C. R.; Weinhold, F. *J. Am. Chem. Soc.* **2006**, *128*, 7335.
(34) Grant, D. J.; Dixon, D. A. *J. Phys. Chem. A* **2006**, *110*, 12955.
(35) Caputo, C. A.; Power, P. P. *Organometallics* **2013**, *32*, 2278.
(36) Haaland, A.; Shorokhov, D. J.; Volden, H. V.; Klinkhammer, K. W. *Inorg. Chem.* **1999**, *38*, 1118.
(37) Klemp, C.; Bruns, M.; Gauss, J.; Häussermann, U.; Stösser, G.; van Wüllen, L.; Jansen, M.; Schnöckel, H. *J. Am. Chem. Soc.* **2001**, *123*, 9099.
(38) Himmel, H.-J.; Vollet, J. *Organometallics* **2002**, *21*, 5972.
(39) Grubisic, A.; Li, X.; Stokes, S. T.; Cordes, J.; Ganteför, G. F.; Bowen, K. H.; Kiran, B.; Jena, P.; Burgert, R.; Schnöckel, H. *J. Am. Chem. Soc.* **2007**, *129*, 5969.
(40) Henke, P.; Pankewitz, T.; Klopper, W.; Breher, F.; Schnöckel, H. *Angew. Chem., Int. Ed.* **2009**, *48*, 8141.
(41) Zhang, X.; Wang, H.; Collins, E.; Lim, A.; Ganteför, G.; Kiran, B.; Schnöckel, H.; Eichhorn, B.; Bowen, K. *J. Chem. Phys.* **2013**, *138*, 124303.
(42) Yang, Z.; Ma, X.; Oswald, R. B.; Roesky, H. W.; Zhu, H.; Schulzke, C.; Starke, K.; Baldus, M.; Schmidt, H.-G.; Noltemeyer, M. *Angew. Chem., Int. Ed.* **2005**, *44*, 7072.
(43) Nakamura, T.; Suzuki, K.; Yamashita, M. *J. Am. Chem. Soc.* **2014**, *136*, 9276.
(44) Wright, R. J.; Phillips, A. D.; Power, P. P. *J. Am. Chem. Soc.* **2003**, *125*, 10784.
(45) Roesky, H. W.; Kumar, S. S. *Chem. Commun.* **2005**, 4027.
(46) Roesky, P. W. *Dalton Trans.* **2009**, 1887.
(47) Schoeller, W. W. *Inorg. Chem.* **2011**, *50*, 2629.
(48) Tan, G.; Szilvási, T.; Inoue, S.; Blom, B.; Driess, M. *J. Am. Chem. Soc.* **2014**, *136*, 9732.
(49) Chu, T.; Korobkov, I.; Nikonov, G. I. *J. Am. Chem. Soc.* **2014**, *136*, 9195.
(50) Ganesamoorthy, C.; Loerke, S.; Gemel, C.; Jerabek, P.; Winter, M.; Frenking, G.; Fischer, R. A. *Chem. Commun.* **2013**, *49*, 2858.
(51) Crimmin, M. R.; Ekkert, O.; White, A. J. P.; Toms, H. *Chem. Sci.* **2015**.
(52) Myers, T. W.; Kazem, N.; Stoll, S.; Britt, R. D.; Shanmugam, M.; Berben, L. A. *J. Am. Chem. Soc.* **2011**, *133*, 8662.
(53) Myers, T. W.; Holmes, A. L.; Berben, L. A. *Inorg. Chem.* **2012**, *51*, 8997.
(54) Myers, T. W.; Berben, L. A. *J. Am. Chem. Soc.* **2013**, *135*, 9988.
(55) Myers, T. W.; Berben, L. A. *Chem. Commun.* **2013**, *49*, 4175.
(56) Berben, L. A. *Chem. - Eur. J.* **2015**, *21*, 2734.
(57) Berben, L. A.; de Bruin, B.; Heyduk, A. F. *Chem. Commun.* **2015**, *51*, 1553.

DOI: 10.1021/jacs.5b05854
J. Am. Chem. Soc. 2015, 137, 10304−10316

(58) Roe, A. L.; Schneider, D. J.; Mayer, R. J.; Pyrz, J. W.; Widom, J.; Que, L., Jr. *J. Am. Chem. Soc.* **1984**, *106*, 1676.
(59) Kau, L. S.; Spira-Solomon, D. J. *J. Am. Chem. Soc.* **1987**, *109*, 6433.
(60) DuBois, J. L.; Mukherjee, P.; Collier, A. M. *J. Am. Chem. Soc.* **1997**, *119*, 8578.
(61) Westre, T. E.; Kennepohl, P.; DeWitt, J. G. *J. Am. Chem. Soc.* **1997**, *119*, 6297.
(62) Aboelella, N. W.; Kryatov, S. V.; Gherman, B. F.; Brennessel, W. W.; Young, V. G.; Sarangi, R.; Rybak-Akimova, E. V.; Hodgson, K. O.; Hedman, B.; Solomon, E. I.; Cramer, C. J.; Tolman, W. B. *J. Am. Chem. Soc.* **2004**, *126*, 16896.
(63) Chaurand, P.; Rose, J.; Briois, V.; Salome, M.; Proux, O.; Nassif, V.; Olivi, L.; Susini, J.; Hazemann, J.-L.; Bottero, J.-Y. *J. Phys. Chem. B* **2007**, *111*, 5101.
(64) Wong, J.; Lytle, F. W.; Messmer, R. P.; Maylotte, D. H. *Phys. Rev. B* **1984**, *30*, 5596.
(65) McKeown, D. A. *Phys. Chem. Miner.* **1989**, *16*, 678.
(66) Li, D. E.; Bancroft, G. M.; Fleet, M. E.; Feng, X. H.; Pan, Y. M. *Am. Mineral.* **1995**, *80*, 432.
(67) Cabaret, D.; Sainctavit, P.; Ildefonse, P.; Flank, A. M. *J. Phys.: Condens. Matter* **1996**, *8*, 3691.
(68) Ildefonse, P.; Cabaret, D.; Sainctavit, P.; Calas, G.; Flank, A. M.; Lagarde, P. *Phys. Chem. Miner.* **1998**, *25*, 112.
(69) Balde, C. P.; Mijovilovich, A. E. *J. Phys. Chem. C* **2007**, *111*, 11721.
(70) Léon, A.; Balerna, A.; Cinque, G.; Frommen, C.; Fichtner, M. *J. Phys. Chem. C* **2007**, *111*, 3795.
(71) Aramburo, L. R.; Liu, Y.; Tyliszczak, T.; de Groot, F. M. F.; Andrews, J. C.; Weckhuysen, B. M. *ChemPhysChem* **2013**, *14*, 496.
(72) van der Bij, H. E.; Cicmil, D.; Wang, J.; Meirer, F.; de Groot, F. M. F.; Weckhuysen, B. M. *J. Am. Chem. Soc.* **2014**, *136*, 17774.
(73) Bearden, J. A.; Burr, A. F. *Rev. Mod. Phys.* **1967**, *39*, 125.
(74) Qian, B.; Ward, D. L.; Smith, M. R. *Organometallics* **1998**, *17*, 3070.
(75) Stender, M.; Eichler, B. E.; Hardman, N. J.; Power, P. P.; Prust, J.; Noltemeyer, M.; Roesky, H. W. *Inorg. Chem.* **2001**, *40*, 2794.
(76) Singh, S.; Ahn, H.-J.; Stasch, A.; Jancik, V.; Roesky, H. W.; Pal, A.; Biadene, M.; Herbst-Irmer, R.; Noltemeyer, M.; Schmidt, H.-G. *Inorg. Chem.* **2006**, *45*, 1853.
(77) Hunziker, W.; Walters, M. R.; Norman, A. W. *J. Biol. Chem.* **1980**, *255*, 9534.
(78) Kaulich, B.; Bacescu, D.; Cocco, D.; Susini, J.; Salome, M.; Dhez, O.; David, C.; Weitkamp, T.; Di Fabrizio, E.; Cabrini, S.; Morrison, G.; Charalambous, P.; Thieme, J.; Wilhein, T.; Kovac, J.; Podnar, M.; Kiskinova, M. *J. Phys. IV* **2003**, *104*, 103.
(79) Bluhm, H.; Andersson, K.; Araki, T.; Benzerara, K.; Brown, G. E.; Dynes, J. J.; Ghosal, S.; Gilles, M. K.; Hansen, H. C.; Hemminger, J. C.; Hitchcock, A. P.; Ketteler, G.; Kilcoyne, A. L. D.; Kneedler, E.; Lawrence, J. R.; Leppard, G. G.; Majzlam, J.; Mun, B. S.; Myneni, S. C. B.; Nilsson, A.; Ogasawara, H.; Ogletree, D. F.; Pecher, K.; Salmeron, M.; Shuh, D. K.; Tonner, B.; Tyliszczak, T.; Warwick, T.; Yoon, T. H. *J. Electron Spectrosc. Relat. Phenom.* **2006**, *150*, 86.
(80) Kaznatcheev, K. V.; Karunakaran, C.; Lanke, U. D.; Urquhart, S. G.; Obst, M.; Hitchcock, A. P. *Nucl. Instrum. Methods Phys. Res., Sect. A* **2007**, *582*, 96.
(81) Prendergast, D.; Galli, G. *Phys. Rev. Lett.* **2006**, *96*, 215502.
(82) Feldman, J.; McLain, S. J.; Parthasarathy, A. *Organometallics* **1997**, *16*, 1514.
(83) Budzelaar, P. H. M.; van Oort, A. B.; Orpen, A. G. *Eur. J. Inorg. Chem.* **1998**, *1998*, 1485.
(84) Burns, C. T.; Shapiro, P. J.; Budzelaar, P. H. M.; Willett, R.; Vij, A. *Organometallics* **2000**, *19*, 3361.
(85) Benn, R.; Rufinska, A. *Angew. Chem., Int. Ed.* **1986**, *25*, 861.
(86) Yang, Y.; Li, H.; Wang, C.; Roesky, H. W. *Inorg. Chem.* **2012**, *51*, 2204.
(87) Cui, C.; Roesky, H. W.; Hao, H. J.; Schmidt, H. G.; Noltemeyer, M. *Angew. Chem., Int. Ed.* **2000**, *39*, 1815.
(88) Minasian, S. G.; Keith, J. M.; Batista, E. R.; Boland, K. S.; Bradley, J. A.; Daly, S. R.; Kozimor, S. A.; Lukens, W. W.; Martin, R. L.; Nordlund, D.; Seidler, G. T.; Shuh, D. K.; Sokaras, D.; Tyliszczak, T.; Wagner, G. L.; Weng, T.-C.; Yang, P. *J. Am. Chem. Soc.* **2013**, *135*, 1864.
(89) La Pierre, H. S.; Minasian, S. G.; Abubekerov, M.; Kozimor, S. A.; Shuh, D. K.; Tyliszczak, T.; Arnold, J.; Bergman, R. G.; Toste, F. D. *Inorg. Chem.* **2013**, *52*, 11650.
(90) Gianetti, T. L.; Nocton, G.; Minasian, S. G. *J. Am. Chem. Soc.* **2013**, *135*, 3224.
(91) Meihaus, K. R.; Minasian, S. G.; Lukens, W. W., Jr. *J. Am. Chem. Soc.* **2014**, *136*, 6056.
(92) Warwick, T.; Andresen, N.; Comins, J. *AIP Conf. Proc.* **2004**, *705*, 458.
(93) Hitchcock, A. P. *aXis2000*, V. 15-Jan-15; McMaster University: Hamilton, Ontario, Canada, 2008; http://unicorn.mcmaster.ca/axis/aXis2000 (accessed May 12, 2014).
(94) Weng, T. C.; Waldo, G. S.; Penner-Hahn, J. E. *J. Synchrotron Radiat.* **2005**, *12*, 506.
(95) George, G. N. *EDG_FIT*. Stanford Synchrotron Radiation Laboratory, Stanford Linear Accelerator: Stanford, CA; 2000.
(96) Minasian, S. G.; Krinsky, J. L.; Williams, V. A.; Arnold, J. *J. Am. Chem. Soc.* **2008**, *130*, 10086.
(97) Hohenberg, P.; Kohn, W. *Phys. Rev.* **1964**, *136*, B864.
(98) Sham, L. J.; Kohn, W. *Phys. Rev.* **1965**, *140*, A1133.
(99) Blochl, P. E. *Phys. Rev. B* **1994**, *50*, 17953.
(100) Kresse, G.; Furthmuller, J. *Phys. Rev. B* **1996**, *54*, 11169.
(101) Perdew, J. P.; Burke, K.; Ernzerhof, M. *Phys. Rev. Lett.* **1996**, *77*, 3865.
(102) Grimme, S. *J. Comput. Chem.* **2006**, *27*, 1787.
(103) England, A. H.; Duffin, A. M.; Schwartz, C. P.; Uejio, J. S.; Prendergast, D.; Saykally, R. J. *Chem. Phys. Lett.* **2011**, *514*, 187.
(104) Pemmaraju, C. D.; Copping, R.; Wang, S.; Janousch, M.; Teat, S. J.; Tyliszcak, T.; Canning, A.; Shuh, D. K.; Prendergast, D. *Inorg. Chem.* **2014**, *53*, 11415.
(105) Giannozzi, P.; Baroni, S.; Bonini, N.; Calandra, M.; Car, R.; Cavazzoni, C.; Ceresoli, D.; Chiarotti, G. L.; Cococcioni, M.; Dabo, I.; Dal Corso, A.; de Gironcoli, S.; Fabris, S.; Fratesi, G.; Gebauer, R.; Gerstmann, U.; Gougoussis, C.; Kokalj, A.; Lazzeri, M.; Martin-Samos, L.; Marzari, N.; Mauri, F.; Mazzarello, R.; Paolini, S.; Pasquarello, A.; Paulatto, L.; Sbraccia, C.; Scandolo, S.; Sclauzero, G.; Seitsonen, A. P.; Smogunov, A.; Umari, P.; Wentzcovitch, R. M. *J. Phys.: Condens. Matter* **2009**, *21*, 395502.
(106) Vanderbilt, D. *Phys. Rev. B* **1990**, *41*, 7892.
(107) Prendergast, D.; Louie, S. G. *Phys. Rev. B* **2009**, *80*, 235126.
(108) Pascal, T. A.; Boesenberg, U.; Kostecki, R.; Richardson, T. J.; Weng, T.-C.; Sokaras, D.; Nordlund, D.; McDermott, E.; Moewes, A.; Cabana, J.; Prendergast, D. *J. Chem. Phys.* **2014**, *140*, 034107.
(109) Körzdörfer, T.; Kümmel, S.; Marom, N.; Kronik, L. *Phys. Rev. B* **2009**, *79*, 201205.
(110) Momma, K.; Izumi, F. *J. Appl. Crystallogr.* **2011**, *44*, 1272.
(111) Tsai, Y.-C. *Coord. Chem. Rev.* **2012**, *256*, 722.
(112) Sudheendra Rao, M. N.; Roesky, H. W.; Anantharaman, G. *J. Organomet. Chem.* **2002**, *646*, 4.
(113) Uhl, W. *Naturwissenschaften* **2004**, *91*, 305.
(114) Jones, C.; Stasch, A. The Chemistry of the Group 13 Metals in the + 1 Oxidation State. In *The Group 13 Metals Aluminium, Gallium, Indium and Thallium: Chemical Patterns and Peculiarities*; Aldridge, S., Downs, A. J., Eds.; John Wiley & Sons, Ltd: Chichester, U.K., 2011; pp 285−341.
(115) Hardman, N. J.; Phillips, A. D.; Power, P. P. In *Group 13 Chemistry—From Fundamentals to Application*; Atwood, D., Shapiro, P. J., Eds.; American Chemical Society: Washington, DC, 2002; pp 2−15.
(116) Yoon, T. H.; Johnson, S. B.; Benzerara, K.; Doyle, C. S.; Tyliszczak, T.; Shuh, D. K.; Brown, G. E. *Langmuir* **2004**, *20*, 10361.
(117) Drisdell, W. S.; Poloni, R.; McDonald, T. M.; Long, J. R.; Smit, B.; Neaton, J. B.; Prendergast, D.; Kortright, J. B. *J. Am. Chem. Soc.* **2013**, *135*, 18183.

DOI: 10.1021/jacs.5b05854
J. Am. Chem. Soc. 2015, 137, 10304−10316

(118) Zegkinoglou, I.; Ragoussi, M.-E.; Pemmaraju, C. D.; Johnson, P. S.; Pickup, D. F.; Ortega, J. E.; Prendergast, D.; de la Torre, G.; Himpsel, F. J. *J. Phys. Chem. C* **2013**, *117*, 13357.
(119) Pascal, T. A.; Wujcik, K. H.; Velasco-Velez, J.; Wu, C.; Teran, A. A.; Kapilashrami, M.; Cabana, J.; Guo, J.; Salmeron, M.; Balsara, N.; Prendergast, D. *J. Phys. Chem. Lett.* **2014**, *5*, 1547.
(120) Minasian, S. G.; Krinsky, J. L.; Rinehart, J. D.; Copping, R.; Tyliszczak, T.; Janousch, M.; Shuh, D. K.; Arnold, J. *J. Am. Chem. Soc.* **2009**, *131*, 13767.
(121) Macdonald, C. L. B.; Cowley, A. H. *J. Am. Chem. Soc.* **1999**, *121*, 12113.
(122) Wells, P. R. *Prog. Phys. Org. Chem.* **1968**, *6*, 111.
(123) Cotton, F. A.; Wilkinson, G. *Advanced Inorganic Chemistry*, 5th ed.; J. Wiley Sons: New York, 1988.
(124) Dohmeier, C.; Mocker, M.; Schnöckel, H.; Lotz, A.; Schneider, U.; Ahlrichs, R. *Angew. Chem., Int. Ed.* **1993**, *32*, 1428.
(125) Shapiro, P. *Coord. Chem. Rev.* **1999**, *189*, 1.
(126) Noyori, R.; Ohkuma, T. *Angew. Chem., Int. Ed.* **2001**, *40*, 40.
(127) Orimo, S.-I.; Nakamori, Y.; Eliseo, J. R.; Zuettel, A.; Jensen, C. M. *Chem. Rev.* **2007**, *107*, 4111.
(128) Sakintuna, B.; Lamari-Darkrim, F.; Hirscher, M. *Int. J. Hydrogen Energy* **2007**, *32*, 1121.
(129) Zidan, R.; Garcia-Diaz, B. L.; Fewox, C. S.; Stowe, A. C.; Gray, J. R.; Harter, A. G. *Chem. Commun.* **2009**, 3717.
(130) Graetz, J.; Reilly, J. J.; Yartys, V. A.; Maehlen, J. P.; Bulychev, B. M.; Antonov, V. E.; Tarasov, B. P.; Gabis, I. E. *J. Alloys Compd.* **2011**, *509*, S517.

DOI: 10.1021/jacs.5b05854
J. Am. Chem. Soc. 2015, 137, 10304−10316